
Article:
Dröge, F., Noakes, F.F., Archer, S.A. et al. (11 more authors) (2021) A dinuclear osmium(II) complex near-infrared nanoscopy probe for nuclear DNA. Journal of the American Chemical Society, 143 (48). pp. 20442-20453. ISSN 0002-7863

https://doi.org/10.1021/jacs.1c10325

A dinuclear osmium(II) complex near-infrared nanoscopy probe for nuclear DNA.

Fabian Dröge,[†] Felicity F. Noakes,[‡§] Stuart A. Archer,[‡#] Sreejesh Sreedharan,[‡▽] Ahtasham Raza,[∥] Craig C Robertson,[‡] Sheila MacNeil,[∥] John W. Haycock,[∥] Heather Carson,[‡] Anthony J.H.M. Meijer,*[‡] Carl G. W. Smythe,[§] Jorge Bernardino de la Serna,[⊥] Benjamin Dietzek-Ivanšić *[†] and Jim A. Thomas*[‡]

[†]Institute of Physical Chemistry, Helmholtzweg 4, 07743 Jena, Germany; Institute of Photonic Technology Jena e.V., Albert-Einstein-Straße 9, 07749 Jena, Germany

[‡]Department of Chemistry and [§]Department of Biomedical Science and [∥]Materials Science & Engineering University of Sheffield, Sheffield, S10 2TN, UK

[⊥]Central Laser Facility, Rutherford Appleton Laboratory, Research Complex at Harwell, Science and Technology Facilities Council, Harwell-Oxford, Didcot OX11 0QX, United Kingdom; National Heart and Lung Institute, Faculty of Medicine, Imperial College London, Sir Alexander Fleming Building, Exhibition Road, London SW7 2AZ, United Kingdom

ABSTRACT: With the aim of developing photostable near-infra red cell imaging probes, a convenient route to the synthesis of heteroleptic Os^{II} complexes containing the $Os(TAP)_2$ fragment is reported. This method was used to synthesize the dinuclear Os^{II} complex, $[\{Os(TAP)_2\}_2tpphz]^{4+}$ (where tpphz - tetrapyrido[3,2-a:2′,3′-c:3″,2″- h:2‴,3‴-j]phenazine and TAP = 1,4,5,8- tetraazaphenanthrene). Using a combination of resonance Raman and time-resolved absorption spectroscopy, as well as computational studies, the excited state dynamics of the new complex were dissected. These studies revealed that, although the complex has several close lying excited states, its near-infra red, NIR, emission (λ_{max} =780 nm) is due to a low-lying Os→TAP based ^{3}MCLT state. Cell-based studies revealed that unlike its Ru^{II} analogue, the new complex is neither cytotoxic nor photocytotoxic. However, as it is highly photostable, live-cell permeant, and displays NIR luminescence within the biological optical window, its properties make it an ideal probe for optical microscopy, demonstrated by its use as a super-resolution NIR STED probe for nuclear DNA.

Introduction

Transition metal complexes are finding increasing applications in medicine. Studies of such complexes were largely instigated by the serendipitous discovery of the therapeutic action of cisplatin.[1,2] However, in the last two decades much interest has focused on ruthenium complexes.[3] Although therapeutic leads that coordinate to biological targets, such as DNA and specific proteins, have been developed[4–8] - and in some cases have entered medical trials[9–12] – research into kinetically inert Ru^{II} complexes has also rapidly expanded. For example, pioneering reports by Meggers and colleagues illustrated how Ru^{II} fragments can be used as inert scaffolds to modulate the properties of biologically and medicinally relevant protein-binding substrates, such as kinase inhibitors.[13–15]

Apart from novel connectivity, Ru^{II} complexes often possess physical properties that can be exploited in a therapeutic context. For instance, redox active complexes can show extremely high cytotoxicity.[16] But perhaps the most generally exploited aspect of these systems is their photochemistry which has led to the identification of potential singlet oxygen sensitizers for photodynamic therapy.[11,17–22] As cancer tissue is frequently hypoxic, complexes that directly photodamage DNA have also been developed as phototherapeutics. For example, coordination of the 1,4,5,8- tetraazaphenanthrene ligand, TAP, to Ru^{II} centers can produce a highly oxidizing Ru→TAP ^{3}MCLT photoexcited state that is capable of directly damaging G-rich DNA through charge transfer processes.[23,24]

The Thomas group has explored many aspects of such research and - although studies on novel mononuclear therapeutics and optical probes have been reported [25–27] - much of this work involves oligonuclear systems. Inter alia, these studies have identified anticancer and antibacterial therapeutic leads with multiple modes of actions,[28–31] and cell probes that can be used as dual function therapeutic/imaging theranostics based on the well-known DNA light-switch effect.[32–34]

Of most relevance to this report is our recent work on the dinuclear complex $[\{Ru(TAP)_2\}_2(tpphz)]^{4+}$, $\mathbf{1}^{4+}$, Figure 1, (TAP = 1,4,5,8- tetraazaphenanthrene, tpphz = tetrapyrido[3,2-a:2′,3′-c:3″,2″- h:2‴,3‴-j]phenazine), which binds to duplex and quadruplex DNA with high affinity[33] As the complex is readily taken up by live cells and the oxidizing Ru→TAP ^{3}MCLT state can be accessed through two-photon absorption, TPA, it displays considerable phototoxicity in hypoxic conditions, even when photoexcited with near infrared, NIR, light.[34]

Another rapidly bourgeoning area of research is the development of new technologies and probes for biological imaging. In this context, the photoexcited states of specific metal complexes have also proved fruitful in the design of optical imaging probes. A huge number of Ru^{II} complexes that image a variety of cellular organelles and

biomolecules have been reported. Most of these studies exploit the ability of polypyridyl ligands to affect both the sub-cellular targeting and photophysical properties of the resultant complexes. However, the emission wavelengths from this class of complexes are usually restricted to a range between ~600-660 nm[25,35–41] whereas, an ideal optical probe for such applications should display emission at lower energies.[42]

The use of near-infra-red luminophores offers several advantages in biological imaging. Due to reduced light scattering effects and minimization of light absorption by water and biomolecules, cells and tissue are most transparent to light wavelengths between 700-1000 nm. Furthermore, this spectral window is also associated with low autofluorescence and minimal phototoxicity.[43,44] For this reason, NIR probes for a variety of fluorescent microscopy techniques are much sought after.[44–46] Although probes for super-resolution methods such as STORM are well established,[47,48] reports on NIR probes that can be used with stimulated emission depletion microscopy (STED) are still rare.

The attraction of STED as a super-resolution technique is that it not only offers sub-diffraction resolutions but is also compatible with optical sectioning and real-time live-cell imaging.[49] However STED probes must also be stable under high photon fluxes as the technique requires both laser excitation and depletion beams.[50,51] In recent years, NIR fluorescent protein tags for STED have been reported. Although these genetically encoded probes can be targeted with high specificity they are bigger, generally dimmer and less photostable than small-molecule luminophores and as a consequence they produce lower spatial and temporal resolutions. [52,53] For these reasons, research into small-molecule based NIR-luminescent dyes for such purposes is undergoing a renaissance.[53,54] Yet, despite the huge interest in these systems, a probe that can image nucleic acids and meet all the criteria required for NIR nanoscopy has yet to be reported. Indeed, SiR-Hoechst (λ_{em} = 672 nm), which was first reported in 2015, is currently the only available far-red emitting DNA stain compatible with STED.[55] However, it displays relatively low brightness compared to typical Hoechst dyes[56] and even when used at low concentrations it is known to induce DNA damage.[57]

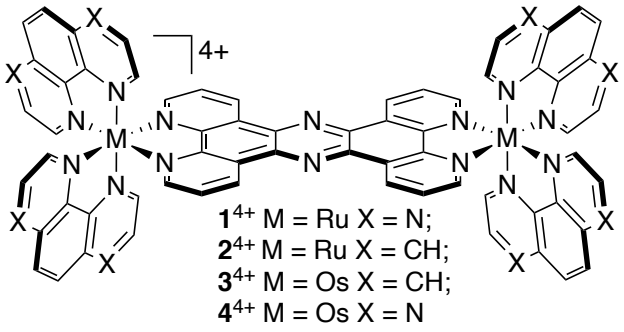

Figure 1. Structure of complexes $\mathbf{1}^{4+}$ - $\mathbf{4}^{4+}$

Due to the aforementioned photo-oxidizing power of the Ru→TAP ^{3}MCLT excited state, a range of ruthenium complexes containing the TAP ligand have reported;[58–60] amongst other things, they have been used to develop novel biological photo-reagents and to explore the charge-transfer properties of DNA.[61–65] Yet, TAP complexes of other metal centers are much less common. In terms of d^6-metal ions, Kirsch-De Mesmaeker and colleagues described the synthesis and optical properties of $[Rh(PPY)_2TAP]^+$ (PPY = phenylpyridine) and related enantiopure derivatives[66] whilst the complexes $[ReX(CO)_3TAP]$ (X= Cl or Br) were reported by the Kaim group as part of a study investigating the lability of Re^I systems[67] but, surprisingly, only one Os^{II} complex with TAP has been reported.

Again, $[Os(TAP)_3]^{2+}$ was reported by the Kirsch-De Mesmaeker group. Due to thermal inaccessibility of its ^{3}MC state, it was found to be more photostable than its Ru^{II} analogue but it is a weaker oxidant due to the lower energy of its Os→TAP ^{3}MCLT excited-state.[68] A striking phenomenon was also identified on comparing the emission properties of $[Os(TAP)_3]^{2+}$ with those of $[Ru(TAP)_3]^{2+}$ and $[Os(phen)_3]^{2+}$ (phen = 1,10 phenanthroline). As expected from many other studies[69–71] the luminescence of $[Os(TAP)_3]^{2+}$ is red-shifted by ~100 nm compared to its Ru^{II} analogue (to 713 nm in water), yet the lifetime and quantum yield for this emission is notably higher than that for $[Os(phen)_3]^{2+}$. Indeed in MeCN, both these terms are considerably larger than those for $[Ru(TAP)_3]^{2+}$ itself. This somewhat unexpected effect is due to a combination of the higher energy of its ^{3}MC state compared to the Ru^{II} complex and a lowered contribution from other non-radiative deactivation pathways compared to $[Os(phen)_3]^{2+}$. In terms of the development of bio-imaging probes, the red-shifted emission on moving from Ru^{II} to Os^{II} is of great interest.[72]

As outlined above, luminophores that emit in the deep-red and near-infrared are attractive platforms for biological imaging as cells and tissue display their greatest transparency at these wavelengths.[73] In previous work, the Thomas group has shown that the complex $[\{Ru(phen)_2\}_2(tpphz)]^{4+}$, $\mathbf{2}^{4+}$ is cell-permeant and can be used as a live-cell imaging probe for nuclear DNA. Thanks to its high photostability, long lifetime, and large Stokes shift, it is also an excellent STED probe.[74]

Although the λ_{max} of this complex is at centered at -670-680 nm, further red-shifting of its luminescence would be advantageous as this would shift its emission further into the biological optical window (650-900 nm). One strategy that has been investigated to accomplish this aim is to substitute Ru^{II} with Os^{II} centers[75,76] and, on first consideration, the use of an Os^{II}-analogue of $\mathbf{2}^{4+}$, may be thought to produce this change. Unfortunately, previous studies have revealed that - thanks to energy gap effects that lead to increased non-radiative deactivation – $\mathbf{3}^{4+}$ is non-emissive at room temperature.[77] However, the observation that $[Os(TAP)_3]^{2+}$ is more emissive than $[Os(phen)_3]^{2+}$ prompted us to investigate the synthesis of $[\{Os(TAP)_2\}_2(tpphz)]^{4+}$, $\mathbf{4}^{4+}$ and compare its photophysical and biological properties with those of $\mathbf{1}^{4+}$ - $\mathbf{3}^{4+}$. Herein, we report that this complex displays radically different photophysical properties to both $\mathbf{1}^{4+}$ and $\mathbf{3}^{4+}$ making it an excellent STED-compatible live-cell probe for visualizing nuclear DNA within the true NIR optical window.

Results and Discussion

Synthesis

Potentially, $\mathbf{4}^{4+}$ could be obtained using the hitherto unreported neutral intermediate $[Os(TAP)_2Cl_2$. This complex would be a suitable starting material for a range of heteroleptic complexes, but as its synthesis is hitherto unreported, we first sought a suitable method for its preparation.

Initially, we attempted to synthesize $[Os(TAP)_2Cl_2]$. through a conventional method commonly used to obtain $[Os(bpy)_2Cl_2]$ first reported by the Meyer group.[78] However - presumably due to the

combination of the kinetically inert nature of the Os center and the electron deficient TAP ligand - this method was unsuccessful.

It is known that microwave mediated heating in closed vessels can decrease reaction times often by multiple orders of magnitude, yielding products that are not accessible by conventional methods. As we found this method to be productive for the synthesis of $\mathbf{1}^{4+}$,[33] we explored the use of microwave mediated heating to obtain $[Os(TAP)_2Cl_2]$. We initially used DMF as a solvent as this is typically used in syntheses of $[M(phen)_2Cl_2]$ (M = Ru and Os). However, we found that under microwave heating appreciable decomposition of DMF to dimethylamine occurs. As the carbon monoxide released in this process binds strongly to Os^{II}, the crude product was a mixture of $[Os(TAP)_2Cl_2]$ and cationic $[Os(TAP)_2(CO)Cl]^+$. Subsequently, it was found that a 1:1 solvent mixture of EtOH and H_2O containing a mixture of $OsCl_3.3H_2O$, TAP, and LiCl led to the precipitation of the required product from the reaction mixture over a period of three hours of microwave heating. After washing with copious amounts of water and diethyl ether $[Os(TAP)_2Cl_2]$ was obtained in high yields (>90%) and purity.

Crude $\mathbf{4}^{4+}$ could then be obtained from the reaction of $[Os(TAP)_2Cl_2]$ and tpphz in similar microwave conditions but over a 9 hour period. Purification of the complex involved a two-step procedure. The first step involved aqueous-organic extraction employing the organic soluble tetrakis(2,5-bis(trifluoromethyl)phenyl borate ($tfpb^-$) anion as a phase-transfer agent. Then ion exchange chromatography was used to produce an analytically pure sample, finally isolated as $[\mathbf{4}]Cl_4$.

To aid identification of spectral features (vide infra), the previously reported $[Os(TAP)_3]^{2+}$ was also resynthesized through the microwave-assisted reaction of $[(NH_4)_2OsCl_6]$ and TAP. Again, the complex was purified by solvent extraction of its $tfpb^-$ salt into dichloromethane.

X-ray quality crystals of both $[Os(TAP)_3]^{2+}$ and $[Os(TAP)_2Cl_2]$ were obtained and structural details are presented in the SI.

Steady state photophysical characterization

The UV-Vis absorption spectrum of $[\mathbf{4}]Cl_4$ in Tris buffer solution can be found in the SI. The compound exhibits a very broad absorption spectrum covering the entire visible range from 350 nm to approximately 750 nm as well as strong absorption in the UV. The UV sections of the spectra are dominated by intense bands assigned to ligand-based ππ* transitions. A distinct absorption feature centered at 360 nm is assigned to tpphz--centered transitions of n–π* character, in accordance to literature reports on closely related Ru^{II} and Os^{II} complexes.[77,79,80] The visible region of the absorption spectrum features a double humped band between 400 - 500 nm that extends out to 750nm. The distinctive spectral shape in the high energy visible regime is very similar to the spectra of $\mathbf{1}^{4+}$ and $\mathbf{2}^{4+}$, however the Ru^{II} complexes lack the low-energy shoulder.

From a consideration of previous studies, the low-energy bands of $\mathbf{4}^{4+}$ are attributed to MLCT transitions. The higher energy double humped band, which is very similar in $\mathbf{1}^{4+}$ - $\mathbf{3}^{4+}$, is due to spin-allowed ^{1}MLCT transitions, hence the higher extinction coefficients. whilst the much less intense, red-shifted, section of the spectrum is assigned to direct excitation into formally forbidden ^{3}MLCT states, which - thanks to the large spin-orbit coupling in Os complexes - is commonly observed for this class of complexes.[81,82] For deeper insights into the MLCT characteristics of the low energy absorption flank, resonance-enhanced Raman (RR) spectroscopy was employed. RR spectra recorded upon excitation across the MLCT portion of the UV-Vis absorption spectrum of $[\mathbf{4}]Cl_4$, is shown in Figure 2. To aid this analysis, similar experiments were also carried out on $[Os(TAP)_3]^{2+}$.

The homoleptic $[Os(TAP)_3]^{2+}$ was investigated at excitation wavelengths of 405 nm, 458 nm and 473 nm – Figure 2. Besides noticeable changes in band intensities at 1410 cm^{-1}, 1593 cm^{-1} and 1627 cm^{-1}, as well as a number of minor changes caused by exciting into different MLCT transitions, the vibrational signature of this complex is marginally altered upon changing the excitation wavelength. This behavior is consistent with the steady state UV-Vis absorption spectra, as well as previous reports on the homoleptic parent complex.

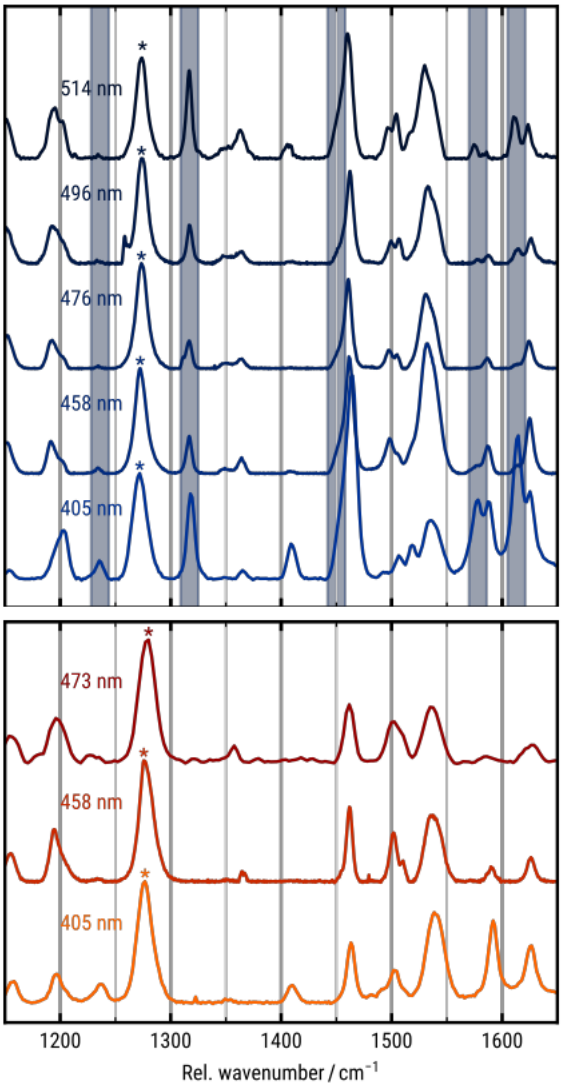

Figure 2. Resonance Raman spectra after background correction at different excitation wavelengths for $[4]Cl_4$ (top), and $[Os(TAP)_3]Cl_2$ (bottom) in Tris buffer. Spectra are normalized to the TAP-centered vibrational band at 1275 cm^{-1} (*). Distinct vibrational features of the heteroleptic complex are highlighted in blue.

Experiments on $\mathbf{4}^{4+}$ were conducted at 405, 458, 473, 476, 496, and 514 nm excitation wavelengths. On changing the excitation wavelength, a number of specific bands display dispersive behavior.

The most pronounced differences are found in the spectrum recorded on excitation at 405nm. This resulted in the increase of bands at 1410 cm^{-1}, 1578 cm^{-1} and 1615 cm^{-1}, which are hardly observed upon excitation at wavelengths > 405 nm. Furthermore, although bands at 1236 cm^{-1}, 1317 cm^{-1} and 1465 cm^{-1} are still present in the spectra excited at wavelengths other than 405 nm they all increase on excitation at this wavelength with respect to the normalization feature at 1275 cm^{-1}.

Comparisons with the spectrum of $[Os(TAP)_3]^{2+}$ revealed that whilst non-dispersive bands are common to both complexes, all the mutable bands involve transitions only observed for $\mathbf{4}^{4}$. This observation indicates that the underlying vibrational modes have contributions from, or are localized on, the coordinated tpphz ligand. Although a band at 1465 cm^{-1} is present in both $[Os(TAP)_3]^{2+}$ and $\mathbf{4}^{4+}$, this feature is significantly more asymmetric and broadened in $\mathbf{4}^{4+}$, indicating that it is a composite of multiple transitions, some of which are localized on the TAP ligand. The decreases in this composite band's intensity at longer wavelengths is hence interpreted as a decrease in contribution from tpphz-based transitions. Besides the intensity changes observed in the high-energy regime, the intensities of other bands, *e.g.*, at 1317 cm^{-1} and 1615 cm^{-1}, regain intensity upon excitation at lower energy wavelengths (≥ 496 nm). This finding indicates that the vibrational structure of the transitions in the low energy MLCT region is similar to those transitions located at around 405 nm.

Taking the above observations into account two conclusions can be drawn. First, the low energy flank of the visible absorption band is dominated by direct singlet-to-triplet MLCT transitions and secondly, the energetic ordering of the participating ligand orbitals is similar in both the singlet and triplet states. This indicates a similar localisation of MLCT transitions in the high and low energy visible absorption bands. We conclude the transitions in the bathochromic section of the spin-allowed absorption appear to be TAP-based ^{1}MLCT in character whereas ^{1}MLCT transitions with large tpphz character are located at the high energy flank of the visible spectrum.

Consistent with the original report,[68] $[Os(TAP)_3]Cl_2$ showed a broad emission between 700–1100 nm and – gratifyingly, and in contrast to $\mathbf{3}^{4+}$ - complex $\mathbf{4}^{4+}$ displayed similar emission behavior. A broad, unstructured emission between 680–1100 nm -with a maximum at around 780 nm (quantum yield; $\Phi = 1.03 \times 10^{-3}$) - resulted upon excitation into the ^{1}MLCT absorption of $\mathbf{4}^{4+}$ (see SI for the steady-state spectrum). Furthermore, apart from a spectral shift of around 70 nm (150 meV), the shapes of the emission spectrum of the heteroleptic complex is very similar to that of its homoleptic parent complex. This indicates a similar emission character for both complexes involving a TAP-centered excited state. Additional evidence toward this conclusion is provided by previous studies on related Ru systems. Ortmans, et al found that - while the paradigm light-switch complex, $[Ru(phen)_2(dppz)]^{2+}$, does not show any emission from aqueous solution - the isostructural $[Ru(TAP)_2(dppz)]^{2+}$ does show strong luminescence in aqueous solution, which was attributed to a TAP centered state as the emissive state.[23] Likewise, whilst $\mathbf{2}^{4+}$ shows no emission in water, as it is excited into a Ru→tpphz ^{3}MCLT state, $\mathbf{1}^{4+}$ and $\mathbf{4}^{4+}$ are luminescent in this solvent as their excited state is M^{II}→TAP ^{3}MCLT in nature.

time resolved spectroscopy

After investigating the steady state spectroscopic properties and the Franck-Condon regime through RR spectroscopy, the question of how the excited state of $\mathbf{4}^{4+}$ is deactivated was addressed, allowing the energy and electron transfer pathways within the new complex to be delineated. Figure 3 show nanosecond and femtosecond resolved transient spectra of $[\mathbf{4}]Cl_4$ in Tris buffer solution. The fs transient absorption spectrum is dominated by a negative signal between 400–700 nm, accompanied by positive differential signals around 350–400 nm and at wavelengths higher than 650 nm. Within a 1600 ps temporal window, these spectral shapes remain nearly constant with a slight intensity decrease in the blue flank of the negative signal around 420 nm for long delay times (>1000 ps). By comparison to the absorption spectrum (blue overlay in figure), the intense negative signal in the visible range is assigned to the ground state bleach (GSB) of $\mathbf{4}^{4+}$.

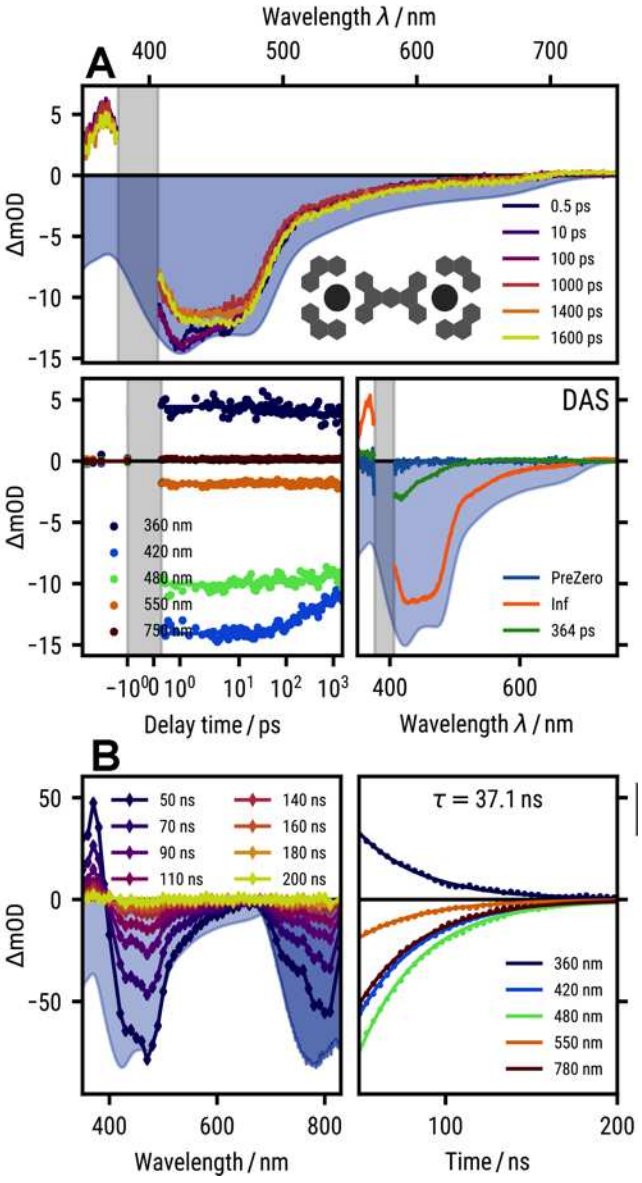

Figure 3. A. Femtosecond time-resolved transient absorption spectra recorded for complexes $[\mathbf{4}]Cl_4$ in aqueous Tris-HCl buffer solution upon excitation at around 400 nm (Top). Associated kinetic traces (bottom left) and resulting decay associated spectra (bottom right). B Nanosecond time resolved transient absorption spectra (Left) Associated selected kinetic traces (right). Experimental data (dots) was fit globally to a single exponential model (solid lines). The blue overlay represents relevant bands in the steady-state absorption spectrum of $[\mathbf{4}]Cl_4$.

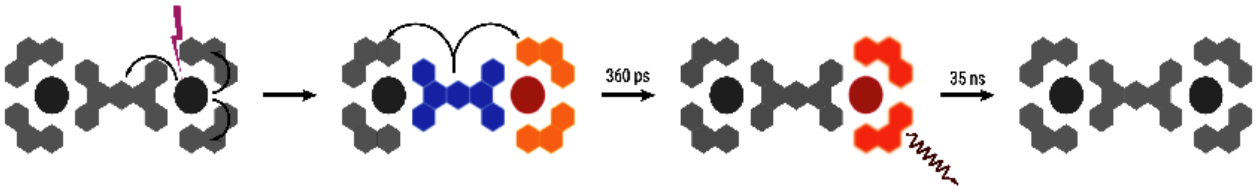

Scheme 1. Model of the excited state dynamics for [**4**]Cl_4

The positive signal in the near UV range, at around 370 nm, is assigned to an excited state absorption (ESA) signal arising from the (partially) negatively charged polypyridyl ligands formed in the MLCT transition. This assignment is in accordance to literature reports on $[Os(bpy)_3]^{2+}$that show a positive transient signal between 340–400 nm, which has been attributed to the ligand anion.[83,84] The weakly positive signal above 650nm is attributed to an ESA signal, localized on the TAP ligand. To quantitatively account for this data, a fit to a single exponential model with a characteristic time component of 360 ps including an infinite lifetime component was required.

The data fit to a monoexponential decay model with a time constant of 37 ns, indicating that the excited state of the complex relaxes through a single decay pathway. The resulting excited-state lifetime is comparable to lifetimes found for structurally similar Os^{II} complexes, such as $[Os(phen)_2(dppz)]Cl_2$, which has a reported emission lifetime of 50 ns.[85] The homoleptic $Os(TAP)_3]^{2+}$ shows similar excited state dynamics and decays to the electronic ground state through a monoexponential decay with an excited state lifetime of 119 ns. These time-resolved experiments offer further evidence that the lowest excited state of [**4**]Cl_4 is an Os→TAP based ^{3}MCLT state, which becomes occupied on irradiation through the mechanism depicted in Scheme 1.

The relatively simple excited state dynamics of the complex might act as a decisive advantage in characterization of its dynamics with more complex biological systems, as potential photochemical conversion processes generated through biomolecular binding will be easily distinguished from the photophysics of the complex itself.

Biophysical studies

Given the DNA binding properties of $\mathbf{1}^{4+}$ and $\mathbf{2}^{4+}$, the interaction of [**4**]Cl_4 with duplex DNA in cell-free conditions was investigated. Steady state UV-Vis titrations revealed characteristic changes in the absorption of the complex on addition of CT-DNA. Initially, the absorption maximum at around 425 nm loses intensity; hypochromism like this is characteristic of a strong interaction between a metal complex and DNA[86] – Figure 4A.

Upon adding more CT-DNA, the absorption band intensity slowly increases homogenously across the visible spectrum. It is known that both $\mathbf{1}^{4+}$ and $\mathbf{2}^{4+}$ bind to duplex with high affinities and the observations for $\mathbf{4}^{4+}$ are consistent with a tight initial bind followed by non-specific binding and/or aggregation. Indeed, these observations are consistent with studies on $\mathbf{2}^{4+}$ which also displays multiple binding modes.[33] Emission spectra recorded over the course of the titration of $\mathbf{4}^{4+}$ with CT-DNA are also consistent with this model – Figure 4B.

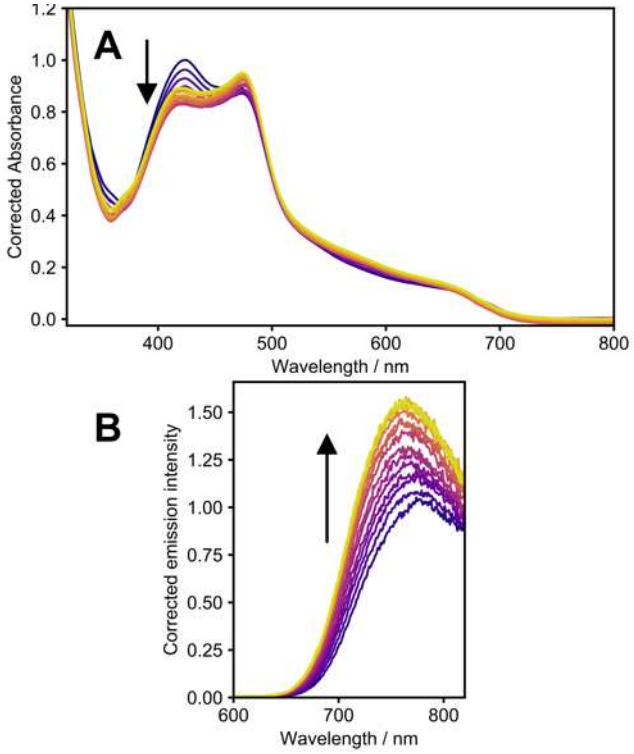

Figure 4. A. Selected spectral changes in the UV-Vis absorption spectrum of [**4**]Cl_4 on addition of CT-DNA. **B**. Equivalent emission changes on addition of CT-DNA. Concentration of complex = 2.11μM

Comparing these changes in emission with those observed in absorption spectra, reveals that the initial decline in absorbance in the 425 nm band correlates with increases in emission. The subsequent hyperchromic shifts in absorption do not correlate with any change in emission, confirming the second phase observed in the absorption titration is due to non-specific interactions. Fits of the absorption changes provide an estimated duplex DNA binding affinity that is identical to that obtained for $\mathbf{1}^{4+}$ ($2 \times 10^6\ M^{-1}$). This is unsurprising as $\mathbf{1}^{4+}$ and $\mathbf{4}^{4+}$ should be virtually structurally identical.

The interaction with CT-DNA also causes a noticeable change in the RR spectral signature of $\mathbf{4}^{4+}$ when excited at 405 nm – Figure 5. The most obvious intensity changes are in energies above 1450 cm^{-1} with distinctive hypochromism found for the bands at 1466 cm^{-1} and 1613 cm^{-1}; although the intensity of the band at 1313 cm^{-1} significantly decreases and slight spectral shifts in bands at 1198 cm^{-1}, 1274 cm^{-1}, 1516 cm^{-1}, 1574 cm^{-1} and 1610 cm^{-1} are also observed. Comparing the relevant features to $[Os(TAP)_3]^{2+}$, a large proportion of the shifted or decreased bands (1198 cm^{-1}, 1274 cm^{-1}, 1313 cm^{-1} and 1574 cm^{-1}) are associated with the

tpphz bridging ligand. As discussed above, comparisons with the homoleptic complex suggests that the bands in the RR spectrum of $\mathbf{4}^{4+}$ at 1465 cm^{-1} and 1610 cm^{-1} are a composite of overlapping tpphz- and TAP-centered vibrational transitions. Their drastically decrease in intensity on addition of DNA indicates that tpphz centered contributions to both of these bands is significantly reduced. In contrast, when the complex is excited at 473 nm, minimal spectral changes occur on addition of CT-DNA. This indicates that the tpphz moiety of $\mathbf{4}^{4+}$ is most affected by the interaction of the complex with DNA.

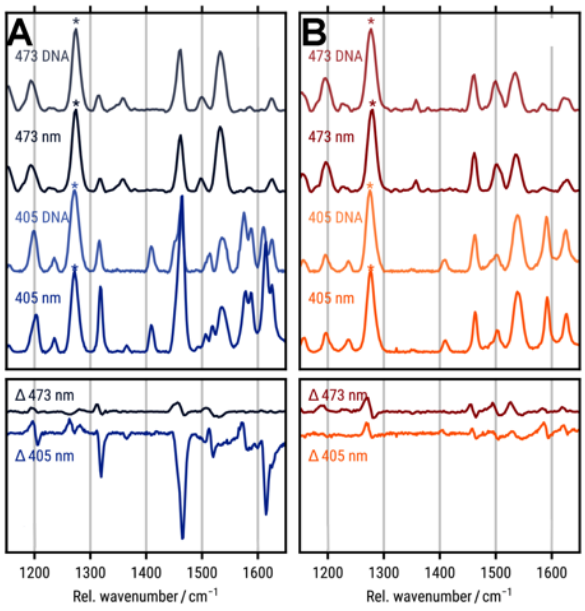

Figure 5. Normalized resonance enhanced Raman spectra (top) and corresponding differential spectra ($I_{DNA} - I_{iso}$, bottom) of $[\mathbf{4}]Cl_4$,(A) and $[Os(TAP)_3]Cl_2$. (B). Numbers besides the sample descriptor indicate the excitation wavelength.

Computational studies

To study complex $\mathbf{4}^{4+}$ in more detail, we performed density functional theory (DFT) calculations as outlined in the experimental section. In these studies, we modeled solvent effects through a continuum solvent model augmented with a small number of explicit water molecules – Figure 6.

As might be expected, the resultant structure, shown in Figure 6a, displays interacting water molecules hydrogen-bonding to the basic nitrogen atoms on the TAP moieties. Interestingly, as observed in related calculations[33] on $\mathbf{1}^{4+}$ it is energetically more advantageous for water molecules to interact with the tpphz moiety as hydrogen bond acceptors, suggesting that the CH groups projecting over the nitrogen atoms on tpphz are basic.

The structure for the triplet state is shown in Figure 6b. Superimposed on this structure is the spin density for the triplet state. As is clear from the image, this density is localized on one of the TAP moieties. This suggests that there may be a number of close-lying triplet states with similar characteristics that are experimentally accessible. Emission from the triplet state is calculated to occur at 713 nm (if a 0–0 transition is assumed; 684 nm, if the emission wavelength is calculated as a difference between the electronic energies for the singlet and triplet states), which is in good agreement with the experimentally observed emission maximum.

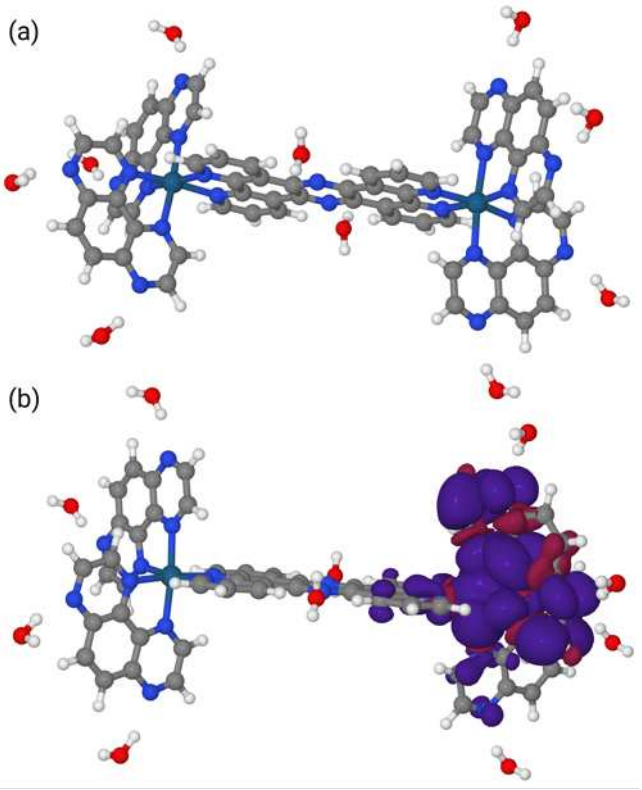

Figure 6: DFT-generated structures for the singlet [panel (a)] and triplet [panel (b) states] of $\mathbf{4}^{4+}$. Panel (b) also includes the spin density associated with the wave function.

The UV-VIS spectra, generated from the calculations using the procedure in the experimental details are shown in Figure 7. It shows an excellent agreement with the experimental data. , when a red-shift of 1000 cm^{-1} is applied to the computational data to account for effects, that are not well accounted for in non-relativistic DFT. Going from $[\mathbf{1}]^{4+}$ to $[\mathbf{4}]^{4+}$ there is a clear red-shift of the spectrum.

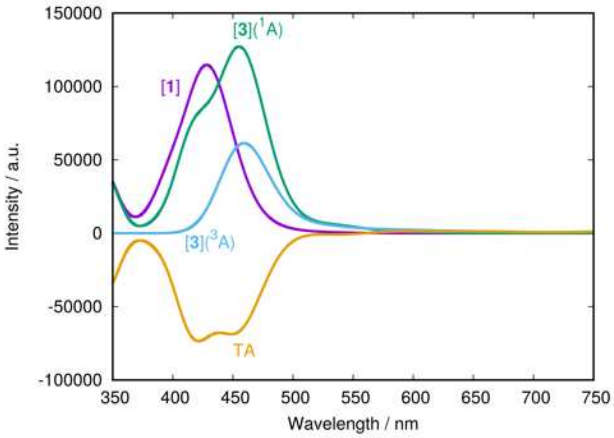

Figure 7: Simulated UV-VIS spectra for $\mathbf{4}^{4+}$ in the singlet ground state and 4^{4+} in the singlet and triplet states. Also shown is the simulated TA spectrum. The calculated spectrum has been red-shifted by 1000 cm^{-1} to align it with the experimental spectrum.

Our calculations do not include spin-orbit coupling and so the direct excitation of the triplet states is not captured. However, our calculations indicate that there is only a single bleach observed in

the TA spectra because the triplet state overlaps with that of the singlet ground state. To investigate the nature of these states in more detail, a wave function analysis was performed on the singlet ground state (see SI for the twelve most intense transitions.) This analysis reveals that all the lowest spin-allowed transitions are excitations onto TAP. Closer analysis of the double-humped feature seen in the absorption spectrum of $\mathbf{4}^{4+}$ shows that it is a mixture of both ^{1}MLCT transitions onto TAP and tpphz as well as π–π* transitions located on the tpphz ligand itself. Finally, the non-resonant Raman spectra for $\mathbf{4}^{4+}$ in both the singlet and triplet state were considered. Comparing the Raman spectra for both states allows an indication of which modes are enhanced in the excited state. Our calculations show that, for example, the signals at 1465 cm^{-1} and 1613 cm^{-1} are associated with vibrational modes on TAP. Given the direction of electron transfer in the triplet state, an enhancement of the intensity for this mode can be expected in the RR spectrum. Therefore, our analysis confirms that the modes at 1198 cm^{-1}, 1274 cm^{-1}, 1313 cm^{-1} and 1574 cm^{-1} are indeed associated with vibrational modes on the tpphz ligand.

Cell studies

Cytotoxicity

The facts that the emission of complex $\mathbf{4}^{4+}$ is considerably red-shifted compared to that of $\mathbf{1}^{4+}$ and is not quenched by DNA indicate that, as expected, the excited state of the Os^{II} complex is much less oxidizing than the ^{3}MLCT of the Ru complex. This was confirmed through a comparison of the cytotoxicity and phototoxicity of complexes $\mathbf{1}^{4+}$, $\mathbf{2}^{4+}$, and $\mathbf{4}^{4+}$. As previously reported, although complex $\mathbf{1}^{4+}$ shows low cytotoxicity it is highly phototoxic toward 2-D and 3-D cell cultures in both one-photon and two-photon excitation regimes. Contrastingly, despite containing coordinated TAP ligands, complex $\mathbf{4}^{4+}$ displays low cytotoxicity *and* phototoxicity – Figure 8.

Cytotoxicity and phototoxicity was assessed using the human ovarian cancer line, A2780. Cells were treated with $\mathbf{4}^{4+}$ at various concentrations ranging from 1 μM to 100 μM for 48 hours and the cell viabilities were determined by an MTT (3-(4,5-dimethylthiazolyl-2)-2,5-diphenyltetrazolium bromide)) assay using cisplatin as a positive control. As can be seen from Fig 10A, under these conditions, the Os^{II} complex displays negligible cytotoxicity, with its IC_{50} >100 μM being over two orders of magnitude higher than cisplatin (IC_{50} = 1.17 μM). However, unlike $\mathbf{1}^{4+}$, A2780 cells exposed to the complex prior to light irradiation also showed no detectable change in viability – Figure 10B. The data reveals that even at high light irradiation the cytotoxicity of $\mathbf{4}^{4+}$ remains low.

Therefore, in terms of photostability, cytotoxicity, and imaging capabilities, the properties of $\mathbf{4}^{4+}$are much closer to those of $\mathbf{2}^{4+}$ than $\mathbf{1}^{4+}$ and $\mathbf{3}^{4+}$, suggesting that it should be an excellent multifunctional cell probe for a variety of optical techniques, including super-resolution STED. However, an advantage of $\mathbf{4}^{4+}$ for such application is that its emission is considerably red shifted compared to $\mathbf{2}^{4+}$ and, as discussed above, probes that display far-red/NIR are much sought as biological imaging agents.[55,73,87] Consequently, using optical microscopy, we investigated the uptake and luminescence of the complex in live cells.

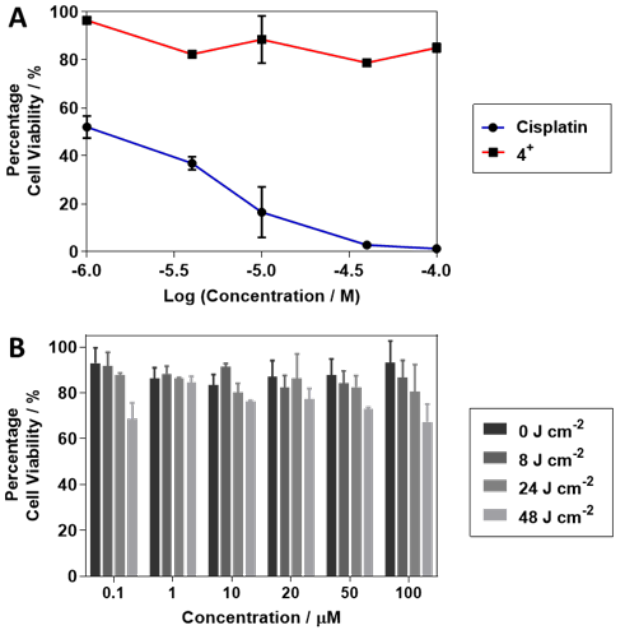

Figure 8. A. Cell viability graph for A2780 cells after treatment with varying concentrations of [**4**]Cl_4 for 48 Hours. Analyzed by an MTT assay with cisplatin employed as a positive control. Experiments performed in triplicate and results given as an average of 2 independent repeats. B. Cell viability graph for A2780 cells after treatment with a concentration gradient of [**4**]Cl_4 and varying light fluences. Experiment performed in triplicate.

High-resolution optical microscope studies

We initially employed the enhanced resolution laser scanner confocal microscope, LSCF, technique AiryScan, which improves lateral resolution so that it is comparable to super-resolution SIM (<140 nm).[88] These studies showed that, like $\mathbf{1}^{4+}$ and $\mathbf{2}^{4+}$, at concentrations above 100 μM, pronounced nuclear staining becomes apparent– Figure 9, although in the case of $\mathbf{4}^{4+}$ emission is now red shifted to >750 nm.

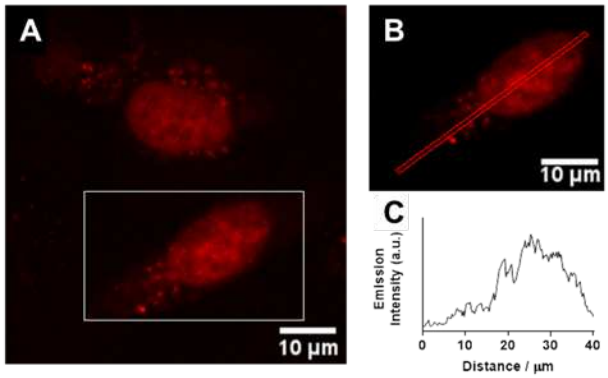

Figure 9. Live cell imaging of MCF7 cells treated with [**4**]Cl_4. A. MCF7 cells treated with 150 μM OsOsTAP for 24 hours. B. Single MCF7 cell and C. Distance vs emission profile of the single cell in B showing nuclear staining.

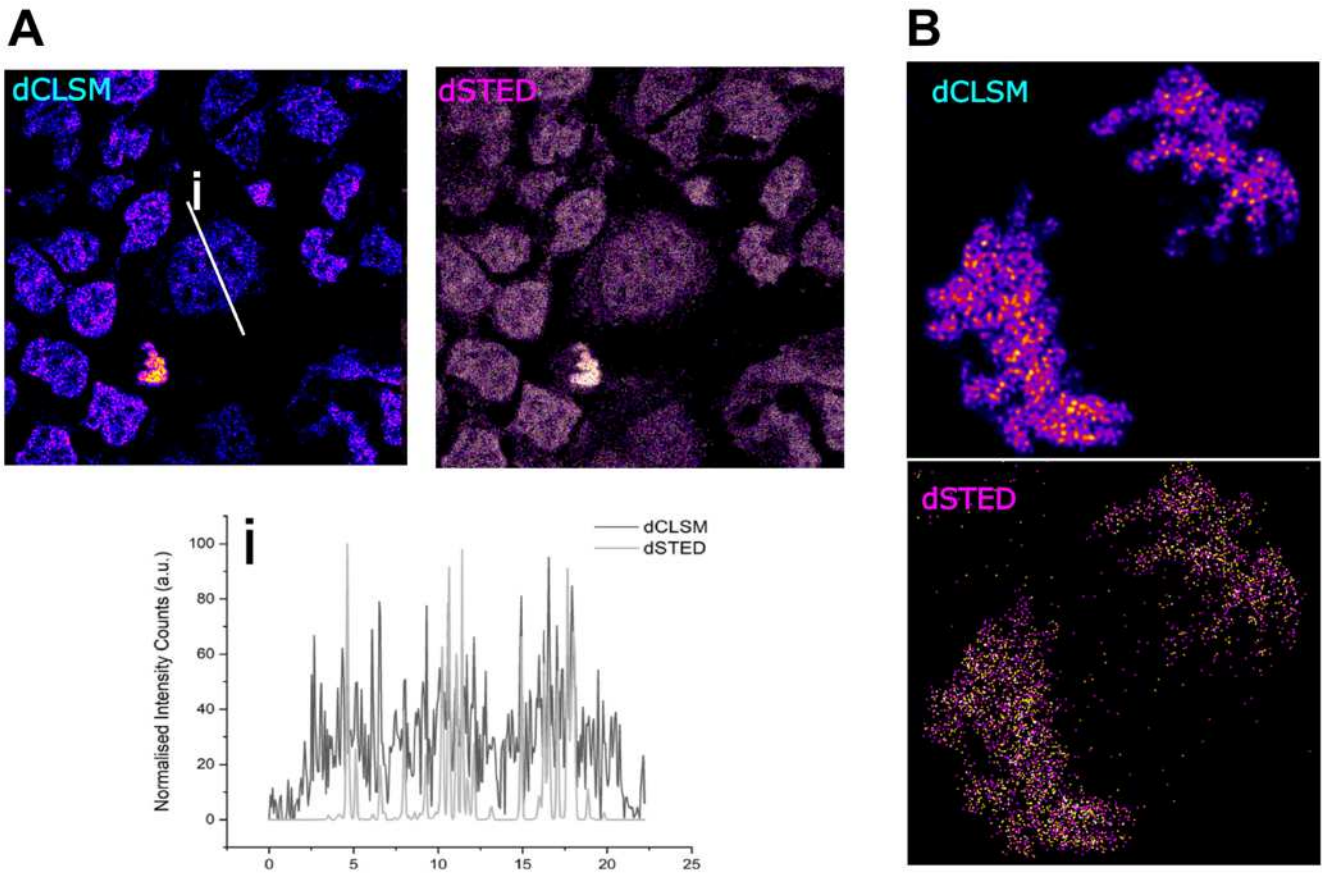

Figure 10: A MCF7 cells treated with 150 μM of[**4**]Cl$_4$.. (**A**) Comparison of CLSM (top left) and STED(top right) data. Bottom left: comparison of CLSM and STED intensity profiles across line (i) drawn on CLSM image. (**B**) Comparison of selected dCLSM (top) and d STED (bottom) image showing a single cell entering mitosis.

As expected, this pattern is similar to that seen in cells treated with its Ru-analogues $\mathbf{1}^{4+}$ and $\mathbf{2}^{4+}$and is attributed to DNA staining. The fact that complexes $\mathbf{1}^{4+}$, $\mathbf{2}^{4+}$, and $\mathbf{4}^{4+}$ display similar localization properties is entirely unsurprising as the structures and charge-density of the complexes are virtually identical. Indeed, several studies have shown that the biological properties of kinetically inert Os^{II} complexes are identical to their Ru^{II} homologues when the metal ions perform a structural function.[70,89–91]

STED Imaging studies

As the photostability and imaging capabilities of $\mathbf{4}^{4+}$ are similar to $\mathbf{2}^{4+}$and the latter complex functions as an excellent optical probe for super-resolution STED,[74] we went on to further investigate the imaging properties of $\mathbf{4}^{4+}$ using this technique and compare it to $\mathbf{1}^{4+}$ and $\mathbf{2}^{4+}$.

As expected, we found that although $\mathbf{1}^{4+}$ can yield STED images, its application is highly restricted due to it potent phototoxicity. Nevertheless, super-resolution images of nuclei in fix cells stained by the complex could be obtained – see SI.

More strikingly, excitation of $\mathbf{4}^{4+}$ leads to images in cells comparable in detail to those obtained with $\mathbf{2}^{4+}$. For example, a comparison with AiryScan CLSM reveals enhanced resolutions with nuclear features being apparent; the increased resolution is further illustrated by the striking differences in intensity plots of nuclear luminescence. – Figure 10A. Images of cells undergoing mitosis are particularly revealing. Planes taken though these cells show chromatin structure in striking detail – Figure 10B. These observations confirm that $\mathbf{4}^{4+}$ functions as a nanoscopy probe for cellular DNA, but with the combined advantages of low phototoxicity and true NIR emission characteristics.

Conclusions

In a previous report, we demonstrated how selective substitution of ancillary ligands within an established DNA binding architecture, led to the identification of a promising phototoxic therapeutic lead, $\mathbf{1}^{4+}$. In this study, through a careful consideration of both ligands and metal ion, we exploit the "modular" composition of this class of heteroleptic transition metal complexes to develop a novel NIR optical probe. This versatility of this approach is illustrated by the fact that while complexes $\mathbf{1}^{4+}$ - $\mathbf{4}^{4+}$ are structurally almost identical, and thus show analogous DNA binding characteristics, their photophysical properties are all radically different; so that, unlikeits Os^{II}-based analogue $\mathbf{3}^{4+}$ which possesses a non-emissive Os→tpphz excited state, complex $\mathbf{4}^{4+}$ displays a Os→TAP ^{3}MCLT excited state that is responsible for its NIR emission.

In our previous report, we demonstrated that one of the most notable features of $\mathbf{2}^{4+}$ as a STED probe is its extreme stability under prolonged laser illumination and complex $\mathbf{4}^{4+}$ is at least as stable; we detected no change in its optical properties during the in-

tense irradiation used in resonance Raman studies and no photobleaching in any of the cellular imaging studies. Indeed as polypyridyl Os^{II} complexes are pronouncedly more kinetically inert than their Ru^{II} analogues, we expect that $\mathbf{4}^{4+}$ may actually more photostable than $\mathbf{2}^{4+}$.

Summing up, the low phototoxicity, high photostability, and long wavelength emission of $\mathbf{4}^{4+}$ means that is ideally suited to be a probe in nanoscopy. In the context of STED, as it exploits a hitherto unused section of the optical spectrum - and it possesses a large Stokes shift, $\mathbf{4}^{4+}$ also offers great potential for multicolor nanoscopy. Studies exploring this possibility -and other multimodal imaging technologies suited to this unique probe - will form the basis of future reports.

ASSOCIATED CONTENT

Supporting Information

The Supporting Information is available free of charge on the ACS Publications website.

Experimental, instrumental, and spectroscopy procedures details; syntheses; cell culture, phototoxicity and cytotoxicity details; UV-vis and luminescent spectra of $\mathbf{4}^{4+}$; CLSM and STED images using $\mathbf{1}^{4+}$; Additional computational data and further references (PDF)

.

AUTHOR INFORMATION

Corresponding Author

*a.meijer@sheffield.ac.uk

*benjamin.dietzek@uni-jena.de

*james.thomas@sheffield.ac.uk

Present Address

[#]Department of Chemistry, Loughborough University, Loughborough, LE11 3TU, UK

[▽]School of Human sciences, University of Derby, Kedleston road, Derby, DE22 1GB, UK.

ACKNOWLEDGMENTS

A license for the OpenEye tools,[92] obtained via the free academic licensing program, is gratefully acknowledged. We are grateful to the EPSRC for postdoctoral funding of S.A.A. and A.R. (EP/M015572/1). FD thanks the EU's ERASMUS+ scheme for financially supporting a visit to Sheffield.

REFERENCES

(1) Rosenberg, B.; Van Camp, L.; Krigas, T. Inhibition Of Cell Division In Escherichia Coli By Electrolysis Products From A Platinum Electrode. *Nature* **1965**, *205*, 698–699.

(2) Rosenberg, B.; Van Camp, L.; Trosko, J. E.; Mansour, V. H. Platinum Compounds: A New Class of Potent Antitumour Agents. *Nature* **1969**, *222* (5191), 385–386.

(3) Gill, M. R.; Thomas, J. A. Ruthenium(II) Polypyridyl Complexes and DNA-from Structural Probes to Cellular Imaging and Therapeutics. *Chem. Soc. Rev.* **2012**, *41* (8), 3179–3192.

(4) Timerbaev, A. R.; Hartinger, C. G.; Aleksenko, S. S.; Keppler, B. K. Interactions of Antitumor Metallodrugs with Serum Proteins:~ Advances in Characterization Using Modern Analytical Methodology. *Chem. Rev.* **2006**, *106* (6), 2224–2248.

(5) Zeng, L.; Gupta, P.; Chen, Y.; Wang, E.; Ji, L.; Chao, H.; Chen, Z.-S. The Development of Anticancer Ruthenium(II) Complexes: From Single Molecule Compounds to Nanomaterials. *Chem. Soc. Rev.* **2017**, *46* (19), 5771–5804.

(6) Murray, B. S.; Babak, M. V; Hartinger, C. G.; Dyson, P. J. The Development of RAPTA Compounds for the Treatment of Tumors . *Coord. Chem. Rev.* **2016**, *306* (P1), 86–114.

(7) Notaro, A.; Gasser, G. Monomeric and Dimeric Coordinatively Saturated and Substitutionally Inert Ru(II) Polypyridyl Complexes as Anticancer Drug Candidates. *Chem. Soc. Rev.* **2017**, *46* (23), 7317–7337..

(8) Licona, C.; Spaety, M.-E.; Capuozzo, A.; Ali, M.; Santamaria, R.; Armant, O.; Delalande, F.; Van Dorsselaer, A.; Cianferani, S.; Spencer, J.; Pfeffer, M.; Mellitzer, G.; Gaiddon, C. A Ruthenium Anticancer Compound Interacts with Histones and Impacts Differently on Epigenetic and Death Pathways Compared to Cisplatin. *Oncotarget* **2017**, *8* (2), 2568–2584.

(9) Trondl, R.; Heffeter, P.; Kowol, C. R.; Jakupec, M. A.; Berger, W.; Keppler, B. K. NKP-1339, the First Ruthenium-Based Anticancer Drug on the Edge to Clinical Application. *Chem. Sci.* **2014**, *5* (8), 2925–2932.

(10) Alessio, E. Thirty Years of the Drug Candidate NAMI-A and the Myths in the Field of Ruthenium Anticancer Compounds: A Personal Perspective. *Eur. J. Inorg. Chem.* **2017**, *2017* (12), 1549–1560.

(11) Heinemann, F.; Karges, J.; Gasser, G. Critical Overview of the Use of Ru(II) Polypyridyl Complexes as Photosensitizers in One-Photon and Two-Photon Photodynamic Therapy. *Acc. Chem. Res.* **2017**, *50* (11), 2727–2736.

(12) Kenny, R. G.; Marmion, C. J. Toward Multi-Targeted Platinum and Ruthenium Drugs - A New Paradigm in Cancer Drug Treatment Regimens? *Chem. Rev.* **2019**, *119* (2), 1058–1137..

(13) Bregman, H.; Carroll, P. J.; Meggers, E. Rapid Access to Unexplored Chemical Space by Ligand Scanning around a Ruthenium Center:~ Discovery of Potent and Selective Protein Kinase Inhibitors. *J. Am. Chem. Soc.* **2006**, *128* (3), 877–884.

(14) Meggers, E. Exploring Biologically Relevant Chemical Space with Metal Complexes. *Curr. Opin. Chem. Biol.* **2007**, *11* (3), 287–292.

(15) Meggers, E. Targeting Proteins with Metal Complexes. *Chem. Commun.* **2009**, *38* (9), 1001–1010.

(16) Notaro, A.; Jakubaszek, M.; Rotthowe, N.; Maschietto, F.; Vinck, R.; Felder, P. S.; Goud, B.; Tharaud, M.; Ciofini, I.; Bedioui, F.; Winter, R. F.; Gasser, G. Increasing the Cytotoxicity of Ru(II) Polypyridyl Complexes by Tuning the Electronic Structure of Dioxo Ligands. *J. Am. Chem. Soc.* **2020**, *142* (13), 6066–6084.

(17) Foxon, S. P.; Alamiry, M. A. H.; Walker, M. G.; Meijer, A. J. H. M.; Sazanovich, I. V; Weinstein, J. A.; Thomas, J. A. Photophysical Properties and Singlet Oxygen Production by Ruthenium(II) Complexes of Benzo[i]Dipyrido[3,2-a:2{\textasciiacute},3{\textasciiacute}- c]Phenazine: Spectroscopic and TD-DFT Study. *J. Phys. Chem. A* **2009**, *113* (46), 12754–12762.

(18) Sun, Y.; Joyce, L. E.; Dickson, N. M.; Turro, C. Efficient DNA Photocleavage by [Ru(Bpy)$_{2}$(Dppn)]$^{2+}$ with Visible Light. *Chem. Commun.* **2010**, *46* (14), 2426.

(19) Mari, C.; Pierroz, V.; Ferrari, S.; Gasser, G. Combination of Ru(II) Complexes and Light: New Frontiers in Cancer Therapy. *Chem. Sci.* **2015**, *6* (5), 2660–2686.

(20) Pierroz, V.; Rubbiani, R.; Gentili, C.; Patra, M.; Mari, C.; Gasser, G. Dual Mode of Cell Death upon the Photo-Irradiation of a RuII Polypyridyl Complex in Interphase or Mitosis. *Chem. Sci.* **2016**, *7* (9), 6115–6124.

(21) Walker, M. G.; Jarman, P. J.; Gill, M. R.; Tian, X.; Ahmad, H.; Reddy, P. A. N.; McKenzie, L.; Weinstein, J. A.; Meijer, A. J. H. M.; Battaglia, G.; Smythe, C. G. W.; Thomas, J. A. A Self-Assembled Metallomacrocycle Singlet Oxygen Sensitizer for Photodynamic Therapy. *Chem. - A Eur. J.* **2016**, *22* (17), 5996–6000.

(22) Liu, J.; Zhang, C.; Rees, T. W.; Ke, L.; Ji, L.; Chao, H. Harnessing Ruthenium(II) as Photodynamic Agents: Encouraging Advances in Cancer Therapy. *Coord. Chem. Rev.* **2018**, *363*, 17–28.

(23) Ortmans, I.; Elias, B.; Kelly, J. M.; Moucheron, C.; Kirsch-

DeMesmaeker, A. [Ru(TAP)2(Dppz)]2+: A DNA Intercalating Complex, Which Luminesces Strongly in Water and Undergoes Photo-Induced Proton-Coupled Electron Transfer with Guanosine-5'-Monophosphate. *Dalton Trans.* **2004**, *2* (4), 668–676. https://doi.org/10.1039/b313213g.

(24) Cloonan, S. M.; Elmes, R. B. P.; Erby, M.; Bright, S. A.; Poynton, F. E.; Nolan, D. E.; Quinn, S. J.; Gunnlaugsson, T.; Williams, D. C. Detailed Biological Profiling of a Photoactivated and Apoptosis Inducing Pdppz Ruthenium(II) Polypyridyl Complex in Cancer Cells. *J. Med. Chem.* **2015**, *58* (11), 4494–4505.

(25) Gill, M. R.; Derrat, H.; Smythe, C. G. W. W.; Battaglia, G.; Thomas, J. A. Ruthenium(II) Metallo-Intercalators: DNA Imaging and Cytotoxicity. *Chembiochem* **2011**, *12* (6), 877–880.

(26) Gill, M. R.; Jarman, P. J.; Halder, S.; Walker, M. G.; Saeed, H. K.; Thomas, J. A.; Smythe, C.; Ramadan, K.; Vallis, K. A. A Three-in-One-Bullet for Oesophageal Cancer: Replication Fork Collapse, Spindle Attachment Failure and Enhanced Radiosensitivity Generated by a Ruthenium(II) Metallo-Intercalator. *Chem. Sci.* **2018**, *9* (4), 841–849.

(27) Smitten, K. L.; Thick, E. J.; Southam, H. M.; de la Serna, J.; Foster, S. J.; Thomas, J. A. Mononuclear Ruthenium(Ii) Theranostic Complexes That Function as Broad-Spectrum Antimicrobials in Therapeutically Resistant Pathogens through Interaction with DNA. *Chem. Sci.* **2020**, *11* (33), 8828–8838.

(28) Saeed, H. K.; Sreedharan, S.; Thomas, J. A. Photoactive Metal Complexes That Bind DNA and Other Biomolecules as Cell Probes, Therapeutics, and Theranostics. *Chem. Commun.* **2020**, *56* (10), 1464–1480.

(29) Jarman, P. J.; Noakes, F.; Fairbanks, S.; Smitten, K.; Griffiths, I. K.; Saeed, H. K.; Thomas, J. A.; Smythe, C. Exploring the Cytotoxicity, Uptake, Cellular Response, and Proteomics of Mono- and Dinuclear DNA Light-Switch Complexes. *J. Am. Chem. Soc.* **2018**, *141* (7), 2925–2937.

(30) Smitten, K. L.; Southam, H. M.; de la Serna, J. B.; Gill, M. R.; Jarman, P. J.; Smythe, C. G. W. W.; Poole, R. K.; Thomas, J. A. Using Nanoscopy to Probe the Biological Activity of Antimicrobial Leads That Display Potent Activity against Pathogenic, Multidrug Resistant, Gram-Negative Bacteria. *ACS Nano* **2019**, *13* (5), 5133–5146.

(31) Smitten, K. L.; Fairbanks, S. D.; Robertson, C. C.; Bernardino De La Serna, J.; Foster, S. J.; Thomas, J. A. Ruthenium Based Antimicrobial Theranostics-Using Nanoscopy to Identify Therapeutic Targets and Resistance Mechanisms in: Staphylococcus Aureus. *Chem. Sci.* **2020**, *11* (1), 70–79.

(32) Saeed, H. K.; Sreedharan, S.; Jarman, P. J.; Archer, S. A.; Fairbanks, S. D.; Foxon, S. P.; Auty, A. J.; Chekulaev, D.; Keane, T.; Meijer, A. J. H. M.; Weinstein, J. A.; Smythe, C. G. W.; Bernardino De La Serna, J.; Thomas, J. A. Making the Right Link to Theranostics: The Photophysical and Biological Properties of Dinuclear RuII-ReI Dppz Complexes Depend on Their Tether. *J. Am. Chem. Soc.* **2020**, *142* (2), 1101–1111

(33) Archer, S. A.; Raza, A.; Dröge, F.; Robertson, C.; Auty, A. J.; Chekulaev, D.; Weinstein, J. A.; Keane, T.; Meijer, A. J. H. M.; Haycock, J. W.; MacNeil, S.; Thomas, J. A. A Dinuclear Ruthenium(Ii) Phototherapeutic That Targets Duplex and Quadruplex DNA. *Chem. Sci.* **2019**, *10*, 3502–3513.

(34) Raza, A.; Archer, S. A.; Fairbanks, S. D.; Smitten, K. L.; Botchway, S. W.; Thomas, J. A.; MacNeil, S.; Haycock, J. W. A Dinuclear Ruthenium(II) Complex Excited by Near-Infrared Light through Two-Photon Absorption Induces Phototoxicity Deep within Hypoxic Regions of Melanoma Cancer Spheroids. *J. Am. Chem. Soc.* **2020**, *142* (10), 4639–4647.

(35) Lo, K. K.-W.; Hui, W.-K.; Chung, C.-K.; Tsang, K. H.-K.; Ng, D. C.-M.; Zhu, N.; Cheung, K.-K. Biological Labelling Reagents and Probes Derived from Luminescent Transition Metal Polypyridine Complexes. *Coord. Chem. Rev.* **2005**, *249* (13–14), 1434–1450.

(36) Puckett, C. A.; Barton, J. K. Methods to Explore Cellular Uptake of Ruthenium Complexes. *J. Am. Chem. Soc.* **2007**, *129* (1), 46–47.

(37) Gill, M. R.; Garcia-Lara, J.; Foster, S. J.; Smythe, C.; Battaglia, G.; Thomas, J. A. A Ruthenium(II) Polypyridyl Complex for Direct Imaging of DNA Structure in Living Cells. *Nat. Chem.* **2009**, *1* (8), 662–667.

(38) Fernández-Moreira, V.; Thorp-Greenwood, F. L.; Coogan, M. P. Application of D6 Transition Metal Complexes in Fluorescence Cell Imaging. *Chem. Commun.* **2009**, *46* (2), 186.

(39) Thomas, J. A. Optical Imaging Probes for Biomolecules: An Introductory Perspective. *Chem. Soc. Rev.* **2015**, *44*, 4494–4500.

(40) Li, G.; Sun, L.; Ji, L.; Chao, H. Ruthenium (Ii) Complexes with Dppz: From Molecular Photoswitch to Biological Applications. *Dalt. Trans.* **2016**, *45*, 13261–13276.

(41) Poynton, F. E.; Bright, S. A.; Blasco, S.; Williams, D. C.; Kelly, J. M.; Gunnlaugsson, T. The Development of Ruthenium(II) Polypyridyl Complexes and Conjugates for I\emph{n Vitro }cellular and \emph{in Vivo} Applications. *Chem. Soc. Rev.* **2017**, *36*, 1–51.

(42) Weissleder, R. A Clearer Vision for in Vivo Imaging. *Nat. Biotechnol.* **2001**, *19* (4), 316–317.

(43) Wäldchen, S.; Lehmann, J.; Klein, T.; van de Linde, S.; Sauer, M. Light-Induced Cell Damage in Live- Cell Super-Resolution Microscopy. *Sci. Rep.* **2015**, *5* (1), 1–12.

(44) Yuan, L.; Lin, W.; Zheng, K.; He, L.; Huang, W. Far-Red to near Infrared Analyte-Responsive Fluorescent Probes Based on Organic Fluorophore Platforms for Fluorescence Imaging. *Chem. Soc. Rev.* **2013**, *42* (2), 622–661.

(45) Luo, S.; Zhang, E.; Su, Y.; Cheng, T.; Shi, C. A Review of NIR Dyes in Cancer Targeting and Imaging. *Biomaterials* **2011**, *32* (29), 7127–7138.

(46) Cheng, Y.; Li, G.; Liu, Y.; Shi, Y.; Gao, G.; Wu, D.; Lan, J.; You, J. Unparalleled Ease of Access to a Library of Biheteroaryl Fluorophores via Oxidative Cross-Coupling Reactions: Discovery of Photostable NIR Probe for Mitochondria. *J. Am. Chem. Soc.* **2016**, *138* (14), 4730–4738.

(47) Lukinavičius, G.; Umezawa, K.; Olivier, N.; Honigmann, A.; Yang, G.; Plass, T.; Mueller, V.; Reymond, L.; Corrêa Jr, I. R.; Luo, Z.-G.; Schultz, C.; Lemke, E. A.; Heppenstall, P.; Eggeling, C.; Manley, S.; Johnsson, K. A Near-Infrared Fluorophore for Live-Cell Super-Resolution Microscopy of Cellular Proteins. *Nat. Chem.* **2013**, *5* (2), 132–139.

(48) Grimm, J. B.; English, B. P.; Chen, J.; Slaughter, J. P.; Zhang, Z.; Revyakin, A.; Patel, R.; Macklin, J. J.; Normanno, D.; Singer, R. H.; Lionnet, T.; Lavis, L. D. A General Method to Improve Fluorophores for Live-Cell and Single-Molecule Microscopy. *Nat. Methods* **2015**, *12* (3), 244–250.

(49) Vicidomini, G.; Bianchini, P.; Diaspro, A. STED Super-Resolved Microscopy. *Nat. Methods* **2018**, *15* (3), 173–182.

(50) Marx, V. Is Super-Resolution Microscopy Right for You? *Nat. Methods* **2013**, *10* (12), 1157–1163.

(51) Kilian, N.; Goryaynov, A.; Lessard, M. D.; Hooker, G.; Toomre, D.; Rothman, J. E.; Bewersdorf, J. Assessing Photodamage in Live-Cell STED Microscopy. *Nat. Methods* **2018**, *15* (10), 755–756.

(52) Fernández-Suárez, M.; Ting, A. Y. Fluorescent Probes for Super-Resolution Imaging in Living Cells. *Nat. Rev. Mol. Cell Biol.* **2008**, *9* (12), 929–943.

(53) Wang, L.; Frei, M. S.; Salim, A.; Johnsson, K. Small-Molecule Fluorescent Probes for Live-Cell Super-Resolution Microscopy. *J. Am. Chem. Soc.* **2018**, *141* (7), 2770–2781.

(54) Lavis, L. D. Chemistry Is Dead. Long Live Chemistry! *Biochemistry* **2017**, *56* (39), 5165–5170.

(55) Lukinavičius, G.; Blaukopf, C.; Pershagen, E.; Schena, A.; Reymond, L.; Derivery, E.; Gonzalez-Gaitan, M.; D'Este, E.; Hell, S. W.; Gerlich, D. W.; Johnsson, K. SiR-Hoechst Is a Far-Red DNA Stain for Live-Cell Nanoscopy. *Nat. Commun.* **2015**, *6*, 8497.

(56) Bucevičius, J.; Keller-Findeisen, J.; Gilat, T.; Hell, S. W.; Lukinavičius, G. Rhodamine-Hoechst Positional Isomers for Highly Efficient Staining of Heterochromatin. *Chem. Sci.* **2019**, *10* (7), 1962–1970.

(57) Sen, O.; Saurin, A. T.; Higgins, J. M. G. The Live Cell DNA Stain SiR-Hoechst Induces DNA Damage Responses and Impairs Cell Cycle Progression. *Sci. Rep.* **2018**, *8* (1), 1–8.

(58) Masschelein, A.; Jacquet, L.; Kirsch-DeMesmaeker, A.; Nasielski, J. Ruthenium Complexes with 1,4,5,8-Tetraazaphenanthrene - Unusual Photophysical Behavior of the Tris-Homoleptic Compound. *Inorg. Chem.* **1990**, *29* (4), 855–860.

(59) Ghesquière, J.; Le Gac, S.; Marcélis, L.; Moucheron, C.; Mesmaeker, A. K.-D. What Does the Future Hold for Photo-Oxidizing Ru(II)

Complexes with Polyazaaromatic Ligands in Medicinal Chemistry? *Curr. Top. Med. Chem.* **2012**, *12* (3), 185–196.

(60) Weynand, J.; Diman, A.; Abraham, M.; Marcélis, L.; Jamet, H.; Decottignies, A.; Dejeu, J.; Defrancq, E.; Elias, B. Towards the Development of Photo-Reactive Ruthenium(II) Complexes Targeting Telomeric G-Quadruplex DNA. *Chem. - A Eur. J.* **2018**, *24* (72), 19216–19227.

(61) Vanderlinden, W.; Blunt, M.; David, C. C.; Moucheron, C.; Kirsch-DeMesmaeker, A.; De Feyter, S. Mesoscale DNA Structural Changes on Binding and Photoreaction with Ru[(TAP) 2PHEHAT] 2+. *J. Am. Chem. Soc.* **2012**, *134* (24), 10214–10221.

(62) Marcélis, L.; Rebarz, M.; Lemaur, V.; Fron, E.; De Winter, J.; Moucheron, C.; Gerbaux, P.; Beljonne, D.; Sliwa, M.; Kirsch-DeMesmaeker, A. Photoaddition of Two Guanine Bases to Single Ru-TAP Complexes. Computational Studies and Ultrafast Spectroscopies to Elucidate the PH Dependence of Primary Processes. *J. Phys. Chem. B* **2015**, *119* (12), 4488–4500.

(63) Kajouj, S.; Marcélis, L.; Lemaur, V.; Beljonne, D.; Moucheron, C. Photochemistry of Ruthenium(Ii) Complexes Based on 1,4,5,8-Tetraazaphenanthrene and 2,2{\textasciiacute}-Bipyrazine: A Comprehensive Experimental and Theoretical Study. *Dalt. Trans.* **2017**, *46* (20), 6623–6633.

(64) Keane, P. M.; O'Sullivan, K.; Poynton, F. E.; Poulsen, B. C.; Sazanovich, I. V.; Towrie, M.; Cardin, C. J.; Sun, X. Z.; George, M. W.; Gunnlaugsson, T.; Quinn, S. J.; Kelly, J. M. Understanding the Factors Controlling the Photo-Oxidation of Natural DNA by Enantiomerically Pure Intercalating Ruthenium Polypyridyl Complexes through TA/TRIR Studies with Polydeoxynucleotides and Mixed Sequence Oligodeoxynucleotides. *Chem. Sci.* **2020**, *11* (32), 8600–8609.

(65) Hall, J. P.; Poynton, F. E.; Keane, P. M.; Gurung, S. P.; Brazier, J. A.; Cardin, D. J.; Winter, G.; Gunnlaugsson, T.; Sazanovich, I. V; Towrie, M.; Cardin, C. J.; Kelly, J. M.; Quinn, S. J. Monitoring One-Electron Photo-Oxidation of Guanine in DNA Crystals Using Ultrafast Infrared Spectroscopy. *Nat. Chem.* **2015**, *7* (12), 961–967.

(66) Didier, P.; Ortmans, I.; Kirsch-De Mesmaeker, A.; Watts, R. J. Electrochemistry and Absorption and Emission Spectroscopy of New Ortho-Metalated Complexes of Rh(III) and Ir(III) with the Ligands 1,4,5,8-Tetraazaphenanthrene and 1,4,5,8,9,12-Hexaazatriphenylene. *Inorg. Chem.* **1993**, *32* (23), 5239–5245.

(67) Klein, A.; Vogler, C.; Kaim, W. The δ in 18 + δ Electron Complexes: Importance of the Metal/Ligand Interface for the Substitutional Reactivity of "Re(0)" Complexes (α-Diimine -)Re I(CO) 3(X). *Organometallics* **1996**, *15* (1), 236–244.

(68) Content, S.; Kirsch-De Mesmaeker, A. A Novel Metallic Complex as Photoreagent for the DNA Guanine Bases: Osmium(II) Tris(Tetraazaphenanthrene). *J. Chem. Soc. Faraday Trans.* **1997**, *93* (6), 1089–1094.

(69) Sauvage, J. P.; Collin, J.-P.; Chambron, J. C.; Guillerez, S.; Coudret, C.; Balzani, V.; Barigelletti, F.; De Cola, L.; Flamigni, L. Ruthenium (II) and Osmium (II) Bis (Terpyridine) Complexes in Covalently-Linked Multicomponent Systems: Synthesis, Electrochemical Behavior, Absorption Spectra, and Photochemical and Photophysical Properties. *Chem. Rev.* **1994**, *94* (4), 993–1019.

(70) Holmlin, R. E.; Barton, J. K. Os(Phen)2(Dppz)2+: A Red-Emitting DNA Probe. *Inorg. Chem.* **1995**, *34* (1), 7–8.

(71) Staffilani, M.; Belser, P.; Hartl, F.; Kleverlaan, C. J.; De Cola, L. Photophysical Properties of Homometallic Ruthenium(II) and Osmium(II) Complexes with a Bis(Dipyridophenazine) Bridging Ligand. From Pico- to Microsecond Time Resolution. *J. Phys. Chem. A* **2002**, *106* (40), 9242–9250.

(72) Zhang, P.; Huang, H. Future Potential of Osmium Complexes as Anticancer Drug Candidates, Photosensitizers and Organelle-Targeted Probes. *Dalt. Trans.* **2018**, *47* (42), 14841–14854.

(73) Hemmer, E.; Benayas, A.; Légaré, F.; Vetrone, F. Exploiting the Biological Windows: Current Perspectives on Fluorescent Bioprobes Emitting above 1000 Nm. *Nanoscale horizons* **2016**, *1* (3), 168–184.

(74) Sreedharan, S.; Gill, M. R.; Garcia, E.; Saeed, H. K.; Robinson, D.; Byrne, A.; Cadby, A.; Keyes, T. E.; Smythe, C.; Pellett, P.; Bernardino De La Serna, J.; Thomas, J. A.; de la Serna, J.; Thomas, J. A. Multimodal Super-Resolution Optical Microscopy Using a Transition-Metal-Based Probe Provides Unprecedented Capabilities for Imaging Both Nuclear Chromatin and Mitochondria. *J. Am. Chem. Soc.* **2017**, *139* (44), 15907–15913.

(75) Byrne, A.; Dolan, C. n; Moriarty, R. D.; Martin, A.; Neugebauer, U.; Forster, R. J.; Davies, A.; Volkov, Y.; Keyes, T. E. Osmium(Ii) Polypyridyl Polyarginine Conjugate as a Probe for Live Cell Imaging; a Comparison of Uptake, Localization and Cytotoxicity with Its Ruthenium(Ii) Analogue. *Dalt. Trans.* **2015**, *44* (32), 14323–14332.

(76) Gkika, K. S.; Noorani, S.; Walsh, N.; Keyes, T. E. Os(II)-Bridged Polyarginine Conjugates: The Additive Effects of Peptides in Promoting or Preventing Permeation in Cells and Multicellular Tumor Spheroids. *Inorg. Chem.* **2021**, *60 (11),*. 8123-8134.

(77) Bolger, J.; Gourdon, A.; Ishow, E.; Launay, J.-P. Mononuclear and Binuclear Tetrapyrido [3, 2-a: 2', 3'-c: 3'', 2''-h: 2''', 3'''-j] Phenazine (Tpphz) Ruthenium and Osmium Complexes. *Inorg. Chem.* **1996**, *35* (10), 2937–2944.

(78) Kober, E. M.; Caspar, J. V; Sullivan, B. P.; Meyer, T. J. Synthetic Routes to New Polypyridyl Complexes of Osmium(II). *Inorg. Chem.* **1988**, *27* (25), 4587–4598.

(79) Bolger, J.; Gourdon, A.; Ishow, E. na; Launay, J.-P. Stepwise Syntheses of Mono- and Di-Nuclear Ruthenium Tpphz Complexes [(Bpy)2Ru(Tpphz)]2? And [(Bpy)2Ru(Tpphz)Ru(Bpy)2]4+{tpphz = Tetrapyrido[3,2-a: 2?,3?-C: 3?,2?-H: 2?,3?-J]Phenazine}. *J. Chem. Soc. Chem. Commun.* **1995**, 1799-1800.

(80) Majewski, M. B.; de Tacconi, N. R.; MacDonnell, frederick M.; Wolf, M. O. Long-Lived, Directional Photoinduced Charge Separation in Ru IIComplexes Bearing Laminate Polypyridyl Ligands. *Chem. - A Eur. J.* **2013**, *19* (25), 8331–8341.

(81) Felix, F.; Ferguson, J.; Güdel, H. U.; Ludi, A. Electronic Spectra of $M(Bipy)_3^{2+}$ Complex Ions (M = Fe, Ru and Os). *Chem. Phys. Lett.* **1979**, *62* (1), 153–157.

(82) Habermehl, J.; Sorsche, D.; Murszat, P.; Rau, S. Making Use of Obstacles: Alternative Synthetic Approaches towards Osmium(II)-Based Photochemical Molecular Devices. *Eur. J. Inorg. Chem.* **2016**, 3423-3428

(83) Shaw, G. B.; Brown, C. L.; Papanikolas, J. M. Investigation of Interligand Electron Transfer in Polypyridyl Complexes of Os(II) Using Femtosecond Polarization Anisotropy Methods: Examination of Os(Bpy)32+ and Os(Bpy)2(Mab)2+. *J. Phys. Chem. A* **2002**, *106* (8), 1483–1495.

(84) Shaw, G. B.; Styers-Barnett, D. J.; Gannon, E. Z.; Granger, J. C.; Papanikolas, J. M. Interligand Electron Transfer Dynamics in [Os(Bpy) 3] 2+: Exploring the Excited State Potential Surfaces with Femtosecond Spectroscopy. *J. Phys. Chem. A* **2004**, *108* (23), 4998–5006..

(85) Holmlin, R. E.; Yao, J. A.; Barton, J. K. Dipyridophenazine Complexes of Os(II) as Red-Emitting DNA Probes: Synthesis, Characterization, and Photophysical Properties. *Inorg. Chem.* **1999**, *38* (1), 174–189..

(86) Long, E. C.; Barton, J. K. On Demonstrating DNA Intercalation. *Acc. Chem. Res.* **1990**, *23* (9), 271–273.

(87) Suseela, Y. V.; Narayanaswamy, N.; Pratihar, S.; Govindaraju, T. Far-Red Fluorescent Probes for Canonical and Non-Canonical Nucleic Acid Structures: Current Progress and Future Implications. *Chem. Soc. Rev.* **2018**, *47* (3), 1098–1131.

(88) Korobchevskaya, K.; Lagerholm, B. C.; Colin-York, H.; Fritzsche, M. Exploring the Potential of Airyscan Microscopy for Live Cell Imaging. *Photonics* **2017**, *4* (3)..

(89) Maksimoska, J.; Williams, D. S.; Atilla-Gokcumen, G. E.; Smalley, K. S. M.; Carroll, P. J.; Webster, R. D.; Filippakopoulos, P.; Knapp, S.; Herlyn, M.; Meggers, E. Similar Biological Activities of Two Isostructural Ruthenium and Osmium Complexes. *Chem. - A Eur. J.* **2008**, *14* (16), 4816–4822.

(90) Mulcahy, S. P.; Meggers, E. Organometallics as Structural Scaffolds for Enzyme Inhibitor Design. *Top. Organomet. Chem.* **2010**, *32*, 141–153.

(91) Wragg, A.; Gill, M. R.; Hill, C. J.; Su, X.; Meijer, A. J. H. M.; Smythe, C.; Thomas, J. A. Dinuclear Osmium(II) Probes for High-Resolution Visualisation of Cellular DNA Structure Using Electron Microscopy . *Chem. Commun.* **2014**, *50*, 14494–14497.

(92) OEChem, Version 2.1.0.; OpenEye Scientific Software, Inc.:, Website: http://www.eyesopen.com. (Accessed 31st Oct 2021)